HYDROLOGIC and LAND SCIENCES APPLICATIONS of NOAA POLAR-ORBITING SATELLITE DATA

UNITED STATES DEPARTMENT OF COMMERCE
National Oceanic and Atmospheric Administration
National Environmental Satellite, Data, and Information Service

Front Cover:

Mount Hood, Oregon
NOAA Photograph

Snow-covered Himalayas
NOAA-6 AVHRR. 22 April 1982.
Visible Image.
Acquired by NOAA/NESDIS, Gilmore, Alaska

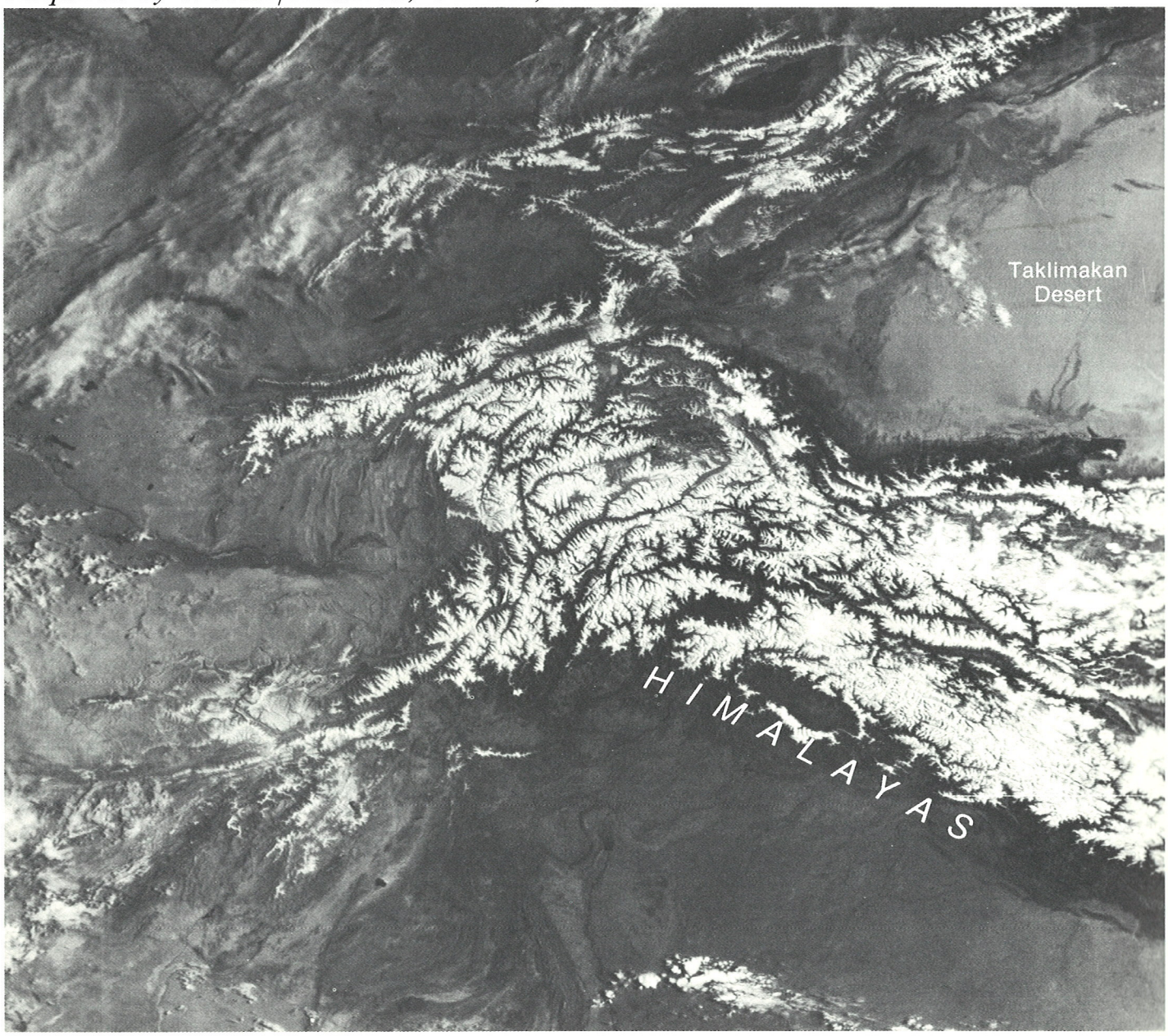

Hydrologic and Land Sciences Applications of NOAA Polar-Orbiting Satellite Data

Contributing Scientists
Michael Matson
Frances Parmenter-Holt

UNITED STATES DEPARTMENT OF COMMERCE
National Oceanic and Atmospheric Administration
National Environmental Satellite, Data, and Information Service
Washington, D.C. 20233

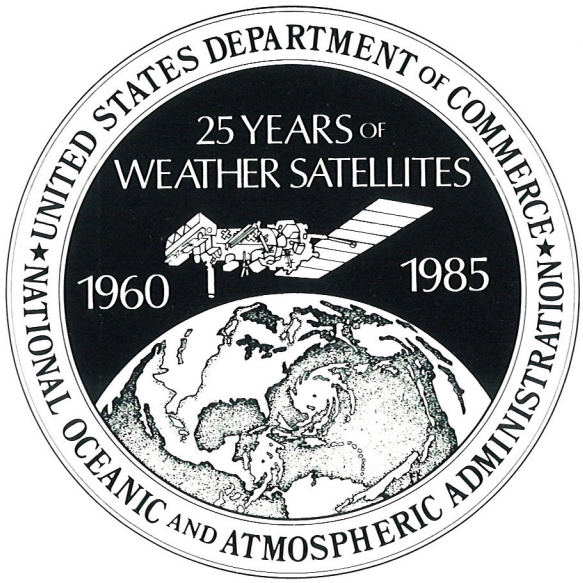

Prepared for:

UNITED STATES DEPARTMENT OF COMMERCE
National Oceanic and Atmospheric Administration
National Environmental Satellite, Data, and Information Service
Washington, D.C. 20233

Under Contract Number NA-83-SAC-00650

By:

THE WALTER A. BOHAN COMPANY

2026 OAKTON STREET, PARK RIDGE, ILLINOIS 60068
APPLIED RESEARCH IN SATELLITE METEOROLOGY AND OCEANOGRAPHY

January 1985

Contents

Introduction 4

Hydrologic Applications 6

Continental Snow Cover 6
Regional Snow Cover Assessment 7
River Basin Snow Mapping 8
River Flood Monitoring 9
Soil Moisture Analysis 10

Renewable Resources 11

Monitoring Vegetation Progress 11
Seasonal Vegetation Changes 12
Fire Fuels Monitoring 13
Fire Detection 15
Fire Monitoring 15

Land Use Analysis 16

Urban Effects 16

Dust and Sandstorm Monitoring 17

Geological Applications 18

Volcanoes 18
Geologic Assessment 19

Epilogue 20

Introduction

The National Environmental Satellite, Data, and Information Service (NESDIS) of the National Oceanic and Atmospheric Administration (NOAA) operates the civil polar-orbiting satellite system for the collection of environmental data. This program began in 1960 with the launch of TIROS-1. Since then, successive satellites in the Improved TIROS Operational Satellite (ITOS) program have grown in sophistication to include concurrent multiple-channel sensing on a daily basis. The latest satellites in the ITOS program are the Advanced TIROS-N spacecraft (4-1) that are renamed NOAA-6, 7, 8, etc., after successful launch.

NOAA satellites are placed in a near-circular, sun-synchronous, near-polar (98.89° inclination), 833- to 870-km high orbit. Approximately fourteen, 102-minute period orbits are made in each 24-hour day. Each orbital view is about 2,700 km wide. The Advanced High Resolution Radiometer (AVHRR) provides both the twice daily view of the globe (Global Area Coverage-GAC) at 4-km resolution and a high resolution (1 km) regional view. Data can be acquired through local, direct readout (High Resolution Picture Transmission-HRPT[1]). For areas beyond the receiving station acquisition circle, data can be tape recorded onboard the spacecraft for delayed readout.

SENSORS

Five channels (see Table 1) of polar-orbiting data can be simultaneously acquired over an area of interest. These data include visible, near-infrared (reflected), and three thermal infrared (emitted) channels. The graphs (5-1) illustrate the location of the AVHRR channels (curve A) relative to the black body curves for solar and terrestrial radiation (curve B) and atmospheric absorption of outgoing radiation (curve C).

The use of data obtained in each channel for hydrology and land sciences is detailed in the succeeding pages and summarized on page 5.

[1] All channels are available in the HRPT broadcast. A 4-km resolution data stream (Automatic Picture Transmission-APT) is also available for direct readout; this is limited to visible and infrared data.

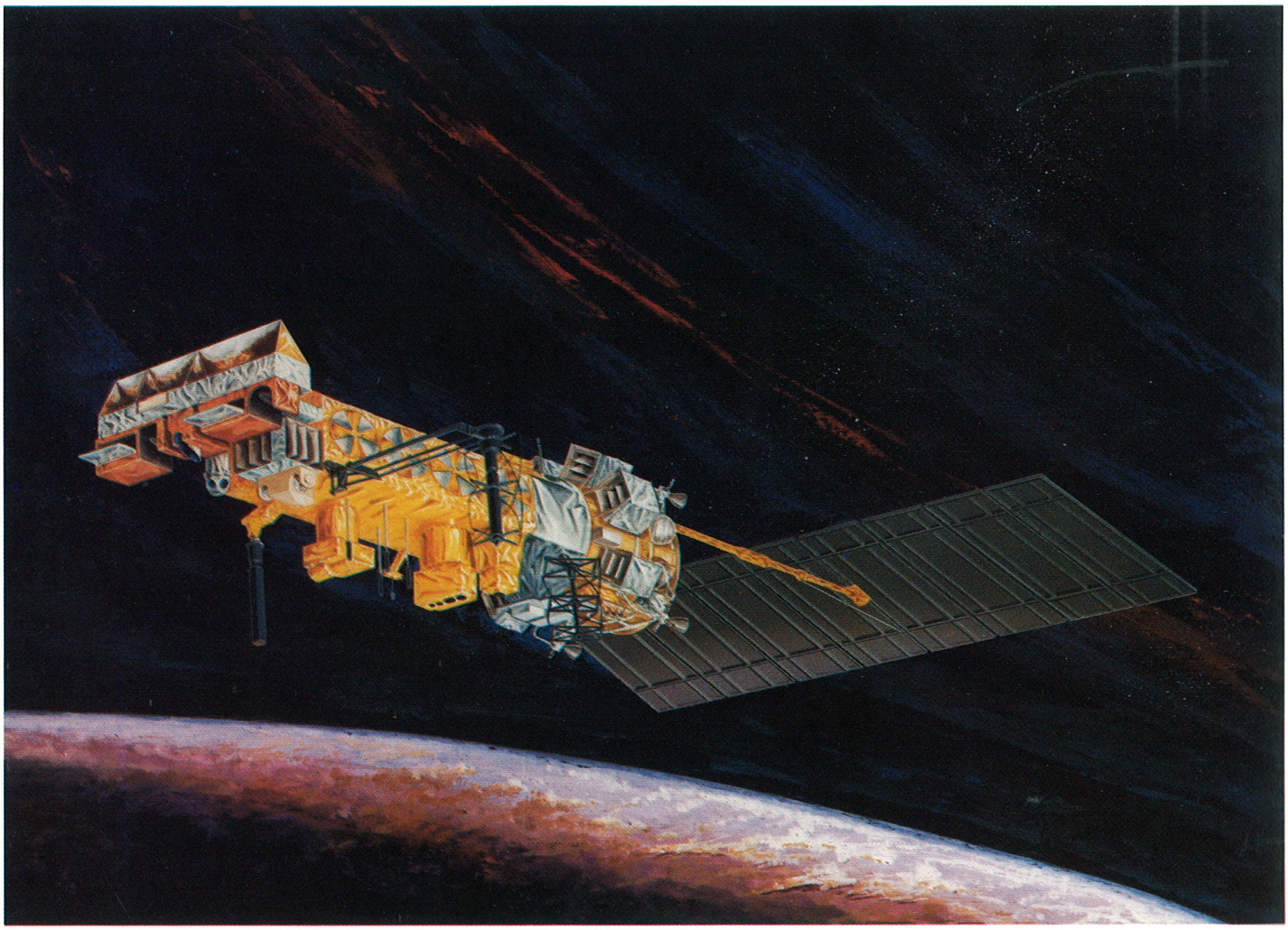

4-1. Artist's conception of the Advanced TIROS-N polar-orbiting environmental satellite. (Courtesy RCA).

TABLE 1 AVHRR SENSORS	
Channel	Wavelengths (μm)
1	0.58 – 0.68
2	0.725 – 1.10
3	3.55 – 3.93
4	10.30 – 11.30
5	11.50 – 12.50

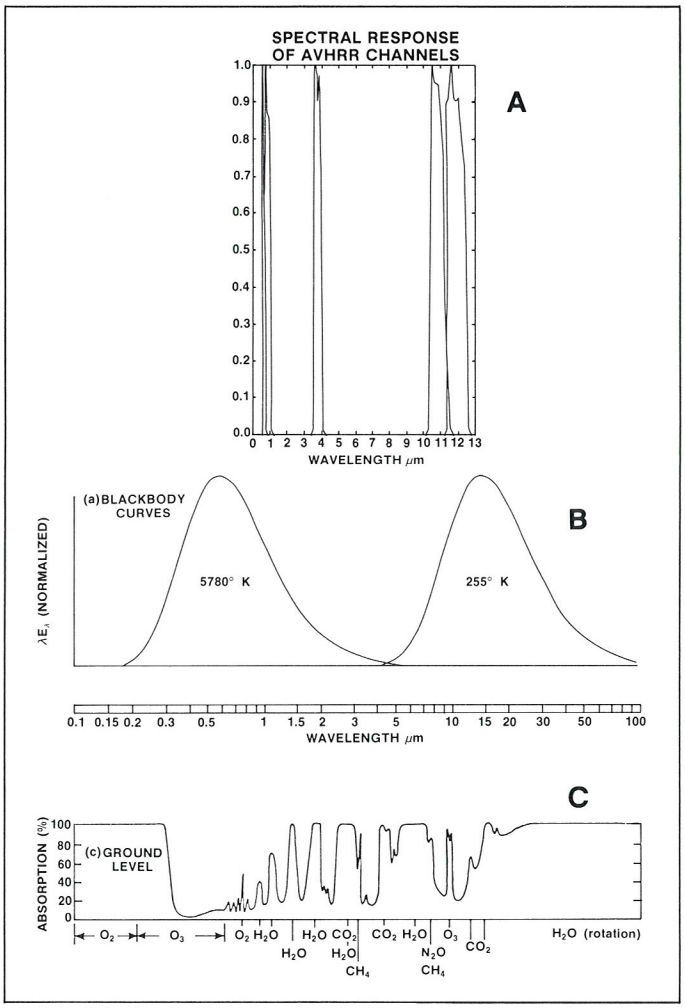

5-1. (a) Spectral response of TIROS-N/NOAA AVHRR channels; (b) Normalized blackbody curves for the sun (5780° K) and the earth (255° K) plotted so that irradiance is proportional to the areas under the curves; (c) Atmospheric absorption in clear air for solar radiation with a zenith angle of 50° and for diffuse terrestrial radiation, (Adapted from R. M. Goody, *Atmospheric Radiation*, Oxford University Press, 1964, p. 4).

Channel 1

Visible, reflected light. Measures albedo; defines snow and ice features; terrain features; vegetative cover; and meteorological (cloud) features.

Channel 2

Near-Infrared, reflected infrared. Defines snow and ice condition and melt; allows vegetation assessment (highly sensitive to the presence of chlorophyll); and meteorological (cloud) monitoring.

Channel 3

Thermal mid-Infrared. Sensitive to extreme heat sources; forest fire detection; sea surface temperature analysis; and nighttime cloud mapping.

Channel 4

Thermal Infrared. Day and night land temperatures; volcanic plumes; meteorological cloud features; and river, lake, and ocean surface temperatures.

Channel 5

Thermal Infrared. Day and night land temperatures; volcanic plumes; meteorological cloud features; and river, lake, and ocean temperatures.

Data recorded in each channel may be used independently or in combination. For example, data from Channels 1 and 2 are used to produce the vegetation index (see page 11) and data from Channels 3, 4, and 5 are used together to filter out cloud and atmospheric water vapor contamination in the analysis of sea surface temperatures.

Depending on the application, these data can be used in a pictorial format or can be analyzed using interactive computer systems. The choice is up to the user. The following pages illustrate the applications of various data formats to the analysis requirements of hydrologists and land scientists. Applications in these scientific disciplines have been steadily growing over the last decade as each new sensor system has been added.

New applications are expected as increasing numbers of users acquire increasingly sophisticated interactive processing systems that will allow for the merging of NOAA satellite data with other satellite, conventional, and geophysical information data sets.

Applications featured in this publication are the development of NOAA, National Aeronautics and Space Administration (NASA), Department of Interior (DOI), and Smithsonian Institution scientists. Only brief descriptions are included here. Additional information may be found by consulting the bibliography at the end of each section.

Further Reading

Allison, L. J., and A. Schnapf, 1983: Meteorological satellites. In *Manual of Remote Sensing*, 2nd Edition, Volume 1, edited by R. N. Colwell, American Society of Photogrammetry, Falls Church, VA, 1232 pp.

Kidwell, K. B., 1984: *NOAA Polar-Orbiter Data (TIROS-N, NOAA-6, NOAA-7, and NOAA-8) Users Guide*. U.S. Dept. of Commerce, NOAA/NESDIS, Washington, D.C., 140 pp.

Lauritson, L., G. J. Nelson, and F. W. Porto, 1979: Data extraction and calibration of TIROS-N/NOAA radiometers. NESS Tech. Memo. 107, U.S. Dept. of Commerce, NOAA/NESS, Washington, D.C., 73 pp.

Schneider, J. R., 1976: Guide for designing RF ground receiving stations for TIROS-N. NESS Tech. Rep. 75, U.S. Dept. of Commerce, NOAA/NESS, Washington, D.C., 117 pp.

Schwalb, A., 1978: The TIROS-N/NOAA A-G satellite series. NOAA Tech. Memo. NESS 95, U.S. Dept. of Commerce, NOAA/NESS, Washington, D.C., 75 pp.

CONTINENTAL SNOW COVER

During the last 25 years climatologists and meteorologists have become more interested in the role of snow cover in climatic processes and weather forecasting. Specifically, snow cover can affect surface and air temperature, atmospheric circulation patterns, storm tracks, cloudiness, surface albedo, radiation balance, evaporation, precipitation, water storage, and soil moisture. Snow cover can also impact energy requirements, transportation systems, food supplies, and the economies of areas dependent on winter recreational facilities.

In order to study and understand the climatic and economic impact of snow cover, it is necessary to have long-period data bases of various snow cover parameters. Of particular interest to users of snow cover data are snow depth and areal snow cover. Snow depth is regularly reported by stations in the World Meteorological Organization network and archived in various data centers. Unfortunately, snow depth observations are limited to point surface measurements, and mountainous and sparsely inhabited areas are poorly represented by conventional data. Until 1966, snow cover analyses were limited to interpolation, temporally and spatially, between these often widely separated points.

In November 1966, the first satellite-derived Northern Hemisphere Weekly Snow and Ice Cover Chart was produced by NESDIS. Since then, continental snow cover has been monitored on a weekly basis using NOAA satellite data. The snow cover data base has been digitized and archived on magnetic tape. In this format several computer-generated products, such as the Northern Hemisphere winter snow cover frequency map (6-1), can be generated.

Further Reading

Dewey, K. F., and R. Heim, Jr., 1982: A digital archive of Northern Hemisphere snow cover, November 1966 through December 1980. *Bull. Amer. Meteor. Soc.*, **63**, 1132–1141.

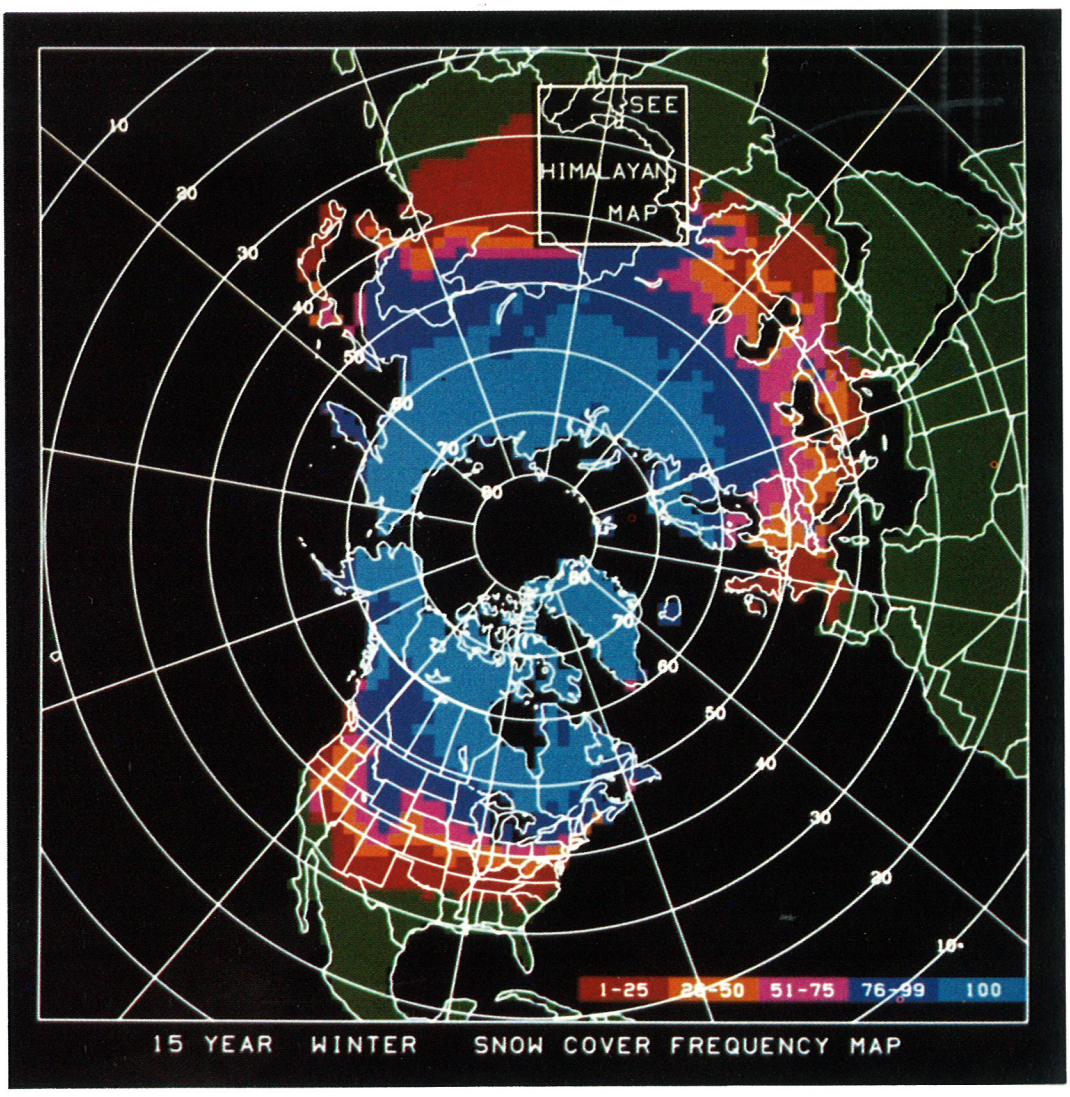

6-1. This map shows the expected frequency of winter snow cover in any part of the Northern Hemisphere based on the historical weekly snow cover data from 1967–1981. The frequency of snow cover is color-coded as follows:

green: 0% (no snow)
red: 1–25%
orange: 26–50%
violet: 51–75%
dark blue: 76–99%
light blue: 100%

Similar maps have been developed for other seasons and for each month of the year.

REGIONAL SNOW COVER ASSESSMENT

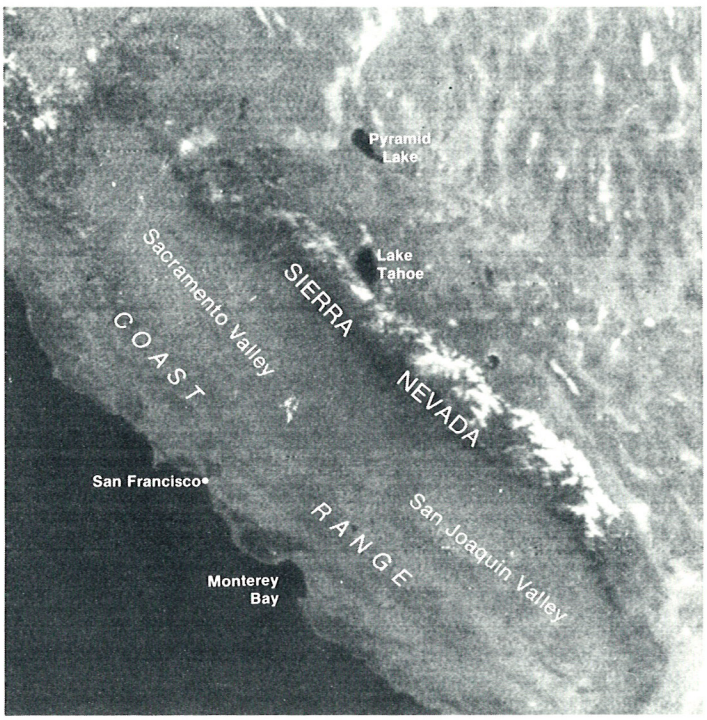

7-1. NOAA-5. Visible Image. 19 April 1977.

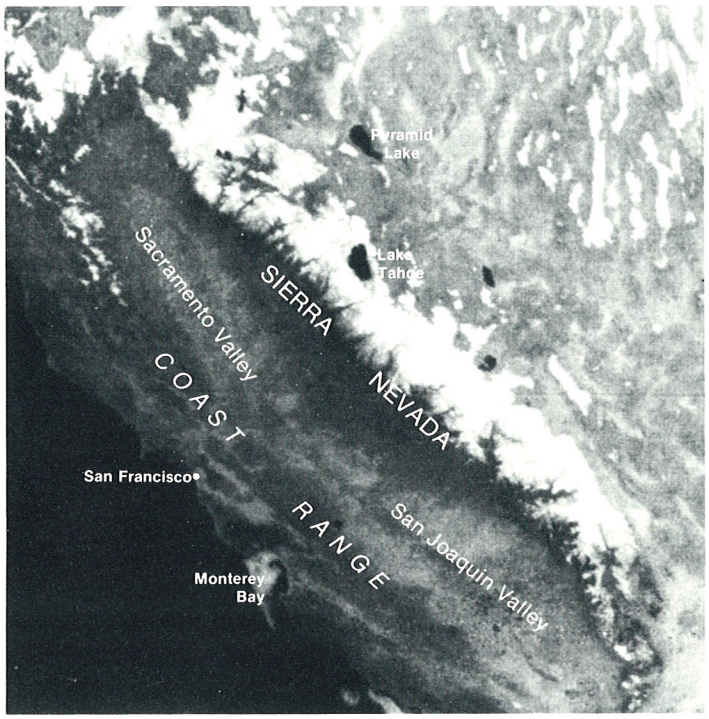

7-2. NOAA-3. Visible Image. 28 April 1975.

Imagery from the NOAA polar-orbiting satellites can be used to assess the extent of snow cover on a regional scale. A striking example occurred during the 1977 drought in California. In that year, the second of two consecutive drought years, California experienced crop devastation, reservoir depletion, water rationing, and widespread timber and brush fires.

Another manifestation of the drought was the record low snow accumulations in the Sierra Nevada, the main source of water for the fertile Sacramento and San Joaquin Valleys. The entire Sierra Nevada range was viewed by the polar-orbiting satellite NOAA-5 on 19 April 1977 (7-1). The bright white areas are the parts of the Sierra Nevada that are snow covered. Cities, lakes and geographical features are annotated on the image for orientation purposes. The Sierra Nevada range was also viewed by NOAA-3 in April 1975, a year of heavy snow (7-2). Areal snow cover measurements for the entire mountain range, derived from the two images, revealed snow cover in 1977 to be one third of that in 1975.

The use of satellite data for snow cover reconnaissance is becoming more widespread in the western United States and in the Sierra Nevada in particular. A cost comparison analysis between satellite and conventional aircraft measurements indicates that the cost of NOAA satellite snow measurements is less than 1% of the cost of aircraft surveys.

Further Reading

Ostrem, G., T. Andersen, and H. Odegaard, 1981: Operational use of satellite data for snow inventory and runoff forecast. In *Satellite Hydrology*, edited by M. Deutsch, D. R. Wiesnet, and A. Rango, American Water Resources Association, Minneapolis, MN, 230–234.

Rango, A., 1984: Operational applications of remote sensing for snow hydrology. In *Renewable Resources Management Applications of Remote Sensing*, American Society of Photogrammetry, Falls Church, VA, 612–633.

Schneider, S. R., and M. Matson, 1977: Satellite observations of snow cover in the Sierra Nevada during the great California drought. *Remote Sensing of Envir.*, **4**, 327–334.

Wiesnet, D. R., and C. P. Berg, 1981: The satellite record of the winter of 1978–79 in North America. In *Satellite Hydrology*, edited by M. Deutsch, D. R. Wiesnet, and A. Rango, American Water Resources Association, Minneapolis, MN, 183–187.

RIVER BASIN SNOW MAPPING

Snow depth and snow-covered area are two important parameters that determine the extent of water runoff in river basins. In many parts of the world this runoff is important for drinking water supplies and irrigation. The NOAA polar-orbiting satellites can not be used to determine snow depth, but they can be used to determine the snow-covered area in a river basin. Snow maps are produced by enlarging and rectifying a visible band image to match the selected river basin map. Registration of the image to the map involves aligning physiographic landmarks such as lakes and rivers, using an optical registration device. The river basin outline is then overlayed on the rectified satellite image. River basins in the Sierra Nevada range are depicted on the NOAA-3 visible image for 28 April 1975 (8-1). The analyst then traces the snow line from the satellite image onto the appropriate basin map. Snow-covered areas can be shaded (8-2), making it easy to electronically or manually calculate the percent of snow-covered area in the basin. The river basin snow condition can then be monitored on a daily, weekly, or monthly basis.

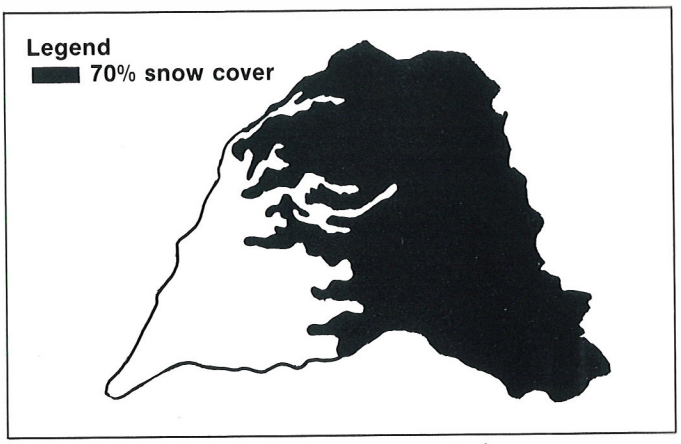

8-2. American River Basin snow-cover analysis.

Further Reading

Bowley, C. J., J. C. Barnes, and A. Rango, 1981: Satellite snow mapping and runoff prediction handbook. NASA Tech. Paper 1829, NASA/GSFC, Greenbelt, MD.

Schneider, S. R., 1981: *Applications Systems Verification and Transfer Project, Volume VI:* Operational applications of satellite snow-cover observations—NOAA/NESS support study. NASA Tech. Paper 1827, NASA/GSFC, Greenbelt, MD, 63 pp.

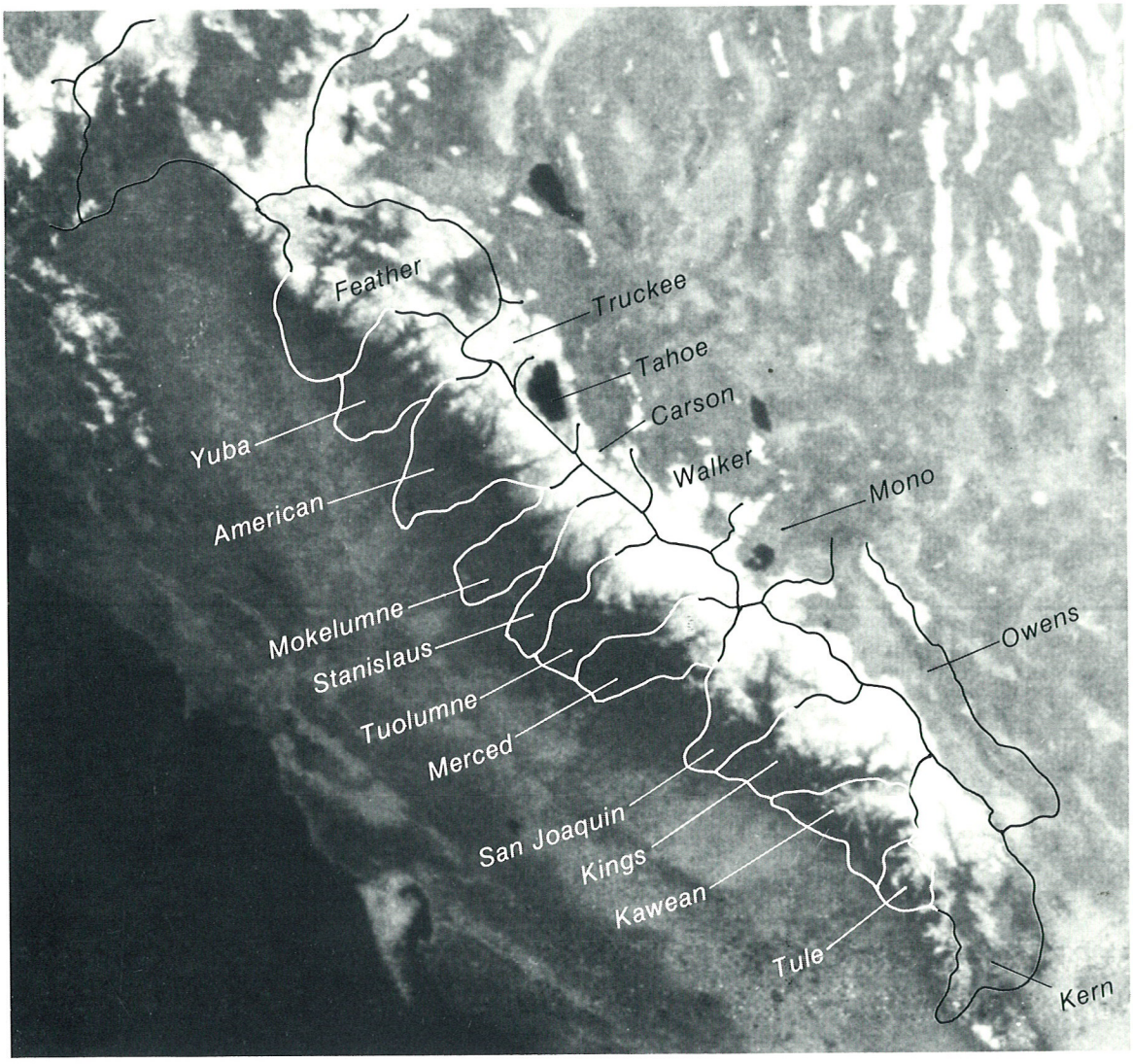

8-1. NOAA-3. Visible Image. 28 April 1975, with superimposed river basin map.

RIVER FLOOD MONITORING

Floods have resulted in death and destruction throughout history. Although construction of flood-preventing structures have helped to protect lives and reduce losses, annual flood losses in the United States often exceed $1 billion. Economics dictate that engineers and government officials be given improved information on the location of flood hazard areas and the assessment of inundated areas when floods occur.

Operational polar-orbiting satellites are a source of this information and have been used in research studies for the 1973 Mississippi River floods, the 1978 Kentucky River, and Red River of the North floods. In each case, the flooded areas showed up best on the nighttime thermal infrared imagery owing to high land/water temperature contrasts.

The AVHRR data reproduced here were used to operationally support NOAA River Forecast Center activities during the 1983 Pearl River floods (9-1). AVHRR thermal infrared satellite imagery of the Pearl River flood were obtained before and during the flood. On 6 March 1983 (9-2), when there was no flooding, the Pearl River was difficult to detect on the satellite picture. However, on 10 April 1983 (9-3), during the height of the spring flood, the river and adjacent water-covered areas were broad and the water temperature was slightly warmer than the land so that the flooded areas stood out prominently.

The flooded areas, observed on satellite data, can be transferred onto a base map of the river and then measured for areal extent. Thus, AVHRR thermal infrared data can be used to monitor both the flood buildup and subsequent abatement.

9-1. Map of Pearl River flood area.

Further Reading

Berg, C. P., and D. F. McGinnis, 1980: Mapping of the 1978 Kentucky River flood from NOAA-5 satellite thermal infrared data. *Proc. 46th Annual Meeting of the American Society of Photogrammetry*, March 9–14, 1980. St. Louis, MO, 106–111.

Berg, C. P., D. R. Wiesnet, and M. Matson, 1981: Assessing the Red River of the North 1978 flooding from NOAA satellite data. In *Satellite Hydrology*, edited by M. Deutsch, D. R. Wiesnet, and A. Rango, American Water Resources Association, Minneapolis, MN, 183–187.

Wiesnet, D. R., D. F. McGinnis, and J. A. Pritchard, 1974: Mapping of the 1973 Mississippi River floods by the NOAA-2 satellite. *Water Resources Bulletin*, **10**, 1040–1049.

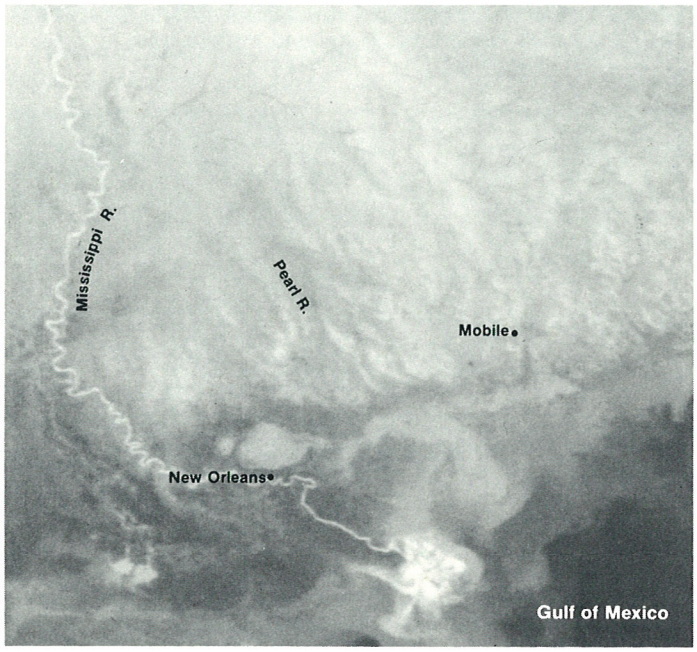

9-2. NOAA-7 AVHRR. 6 March 1983. Pearl River before flooding.

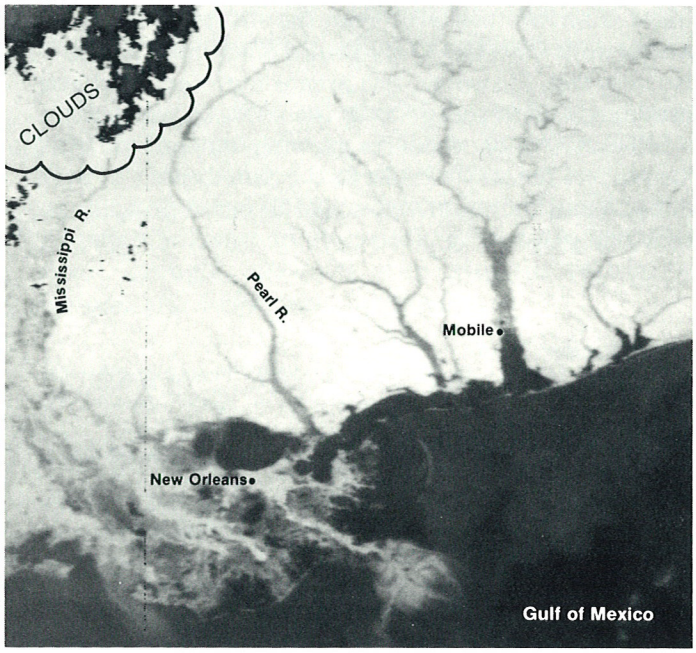

9-3. NOAA-7 AVHRR. 10 April 1983. Pearl River during flooding.

SOIL MOISTURE ANALYSIS

Terrain and soil characteristics are of interest to agriculturists, urban planners, and engineers. The spatial resolution of the NOAA satellite data does not allow for small area assessments (<500 acres), however, the twice daily view by the NOAA spacecraft provides a daytime and nighttime look, clouds permitting, on the regional scale.

Examining characteristics of soils can be done through the use of thermal infrared or the vegetation index (VI). Refer to next section (page 11) for a discussion of the vegetation index. Typically, heavy soils retain moisture far longer than fine, sandy soils, and this difference is best revealed in afternoon infrared imagery. Under similar meteorological conditions, moist soils will appear cooler in infrared imagery than well-drained soils. This can be seen in the afternoon infrared imagery over the Upper and Middle Mississippi Valley (10-1). Notice that the Mississippi River, which marks the eastern boundary of Iowa, and the Des Moines, Iowa, Cedar, and Illinois Rivers appear much cooler than the surrounding land. Slightly warmer surface temperatures (medium gray shades) occur in west-central Wisconsin (A) and northern Missouri (B). Much warmer surface temperatures (dark gray shades) are located over west-central Illinois (C), and extend westward to north-central Iowa (D–E).

Another approach is to examine the vegetation index (VI) display (10-2). This VI display of central and western Iowa shows a large bare soil area (F, dark brown), surrounded by various shades of green that denote green vegetation. The bare soils are phaezoms, associated with gley soils that are dark in color and poorly drained. In the spring, these soils are wetter, colder, and less workable than the surrounding loess-derived soils (G). The Des Moines River bottom (H) is also very wet. However, this area is used for forest and grassland, and at this point in the growing season, it is in full leaf, which obscures viewing the soil surface. The map of Iowa (10-3) shows the distribution of bare soils (F) and loess-derived soils (G) corresponding to the VI display.

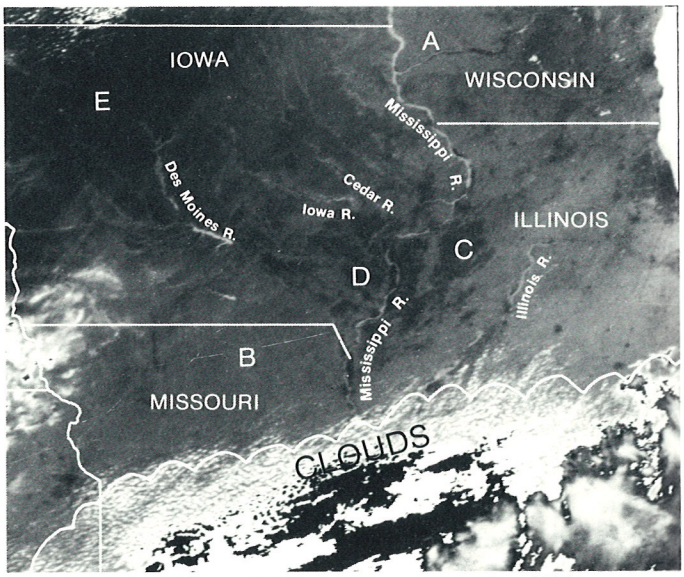

10-1. NOAA-7. Thermal Infrared Image. 15 May 1983.

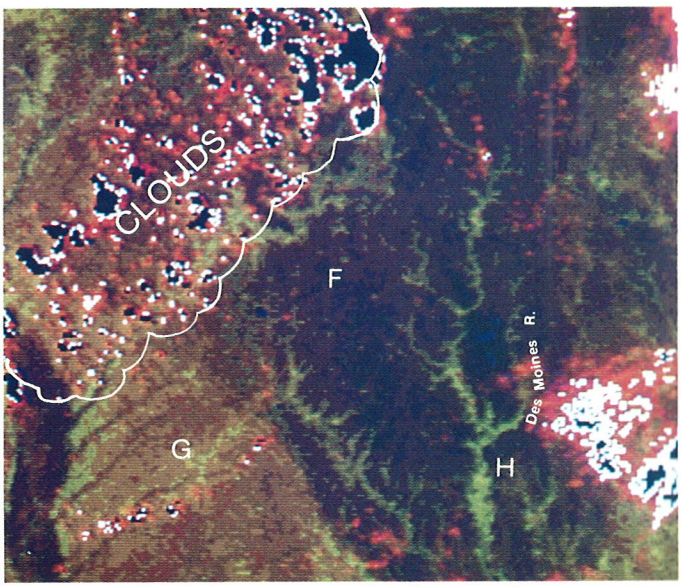

10-2. Vegetation Index over central and western Iowa, 27 May 1983 (from van Dyk et al, 1984).

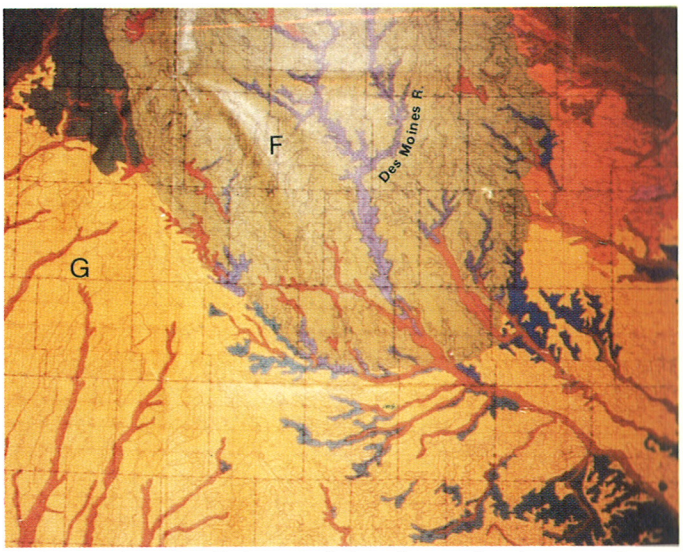

10-3. Terrain and soil characteristics of central and western Iowa.

Further Reading

Heilman, J. L., and D. G. Moore, 1980: Thermography for estimating developing crop canopies. *J. Appl. Meteor.*, **19**, 324–328.

Schmugge, T. J., 1978: Remote sensing of surface soil moisture. *J. Appl. Meteor.*, **17**, 1549–1557.

van Dyk, A., D. McCrary, S. LeDuc, and M. Lyn, 1984: *AVHRR Training Set, Volume 1.* NOAA/NESDIS/AISC and University of Missouri, Columbia, MO, 97 pp.

Vlcek, J., and D. King, 1983: Detection of subsurface soil moisture by thermal sensing: results of laboratory, close range and aerial studies. *Photogrammetric Engineering & Remote Sensing*, **49**, 1593–1597.

MONITORING VEGETATION PROGRESS

Visible and near-infrared sensors, Channels 1 and 2, respectively, onboard the NOAA satellites provide the capability to globally or locally monitor the progress of vegetation. This capability keys on the difference between the reflectance of chlorophyll in green leaves in the visible and near-infrared spectral bands of the onboard sensors. Preliminary use of the differential reflectance data from these spectral regions was demonstrated with the Landsat multispectral data which were used to classify land cover and estimate crop acreage. Similar activities are now ongoing using the NOAA satellite data.

Green vegetation is observed to have a reflectance (albedo) of 20% or less in the visible and up to 60% in the near-infrared. This reflectance changes slightly as crops develop and mature (11-1).

CROP VIGOR FROM NOAA SATELLITE IMAGERY

Channel 2 (Near IR) Minus Channel 1 (Visible)

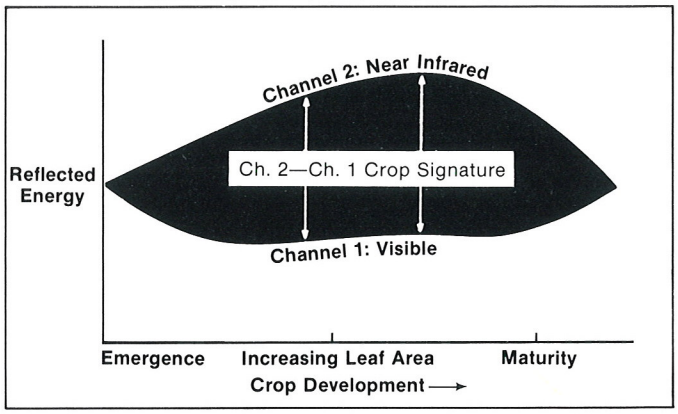

11-1. Visible and near-infrared observed reflected energy of green leafed vegetation. (Adapted from Ambroziak, 1984).

Various mathematical treatments of the data have been explored and have been found responsive to changes in green vegetation. Two vegetation indices have been regularly calculated from the NOAA satellite data. The simplest vegetation index (VI) is the result of the difference between Channel 2 and 1:

$$\mathbf{VI = Channel\ 2 - Channel\ 1}$$

A normalized vegetation index (NVI) is the ratio of the VI and the sum of Channels 2 and 1:

$$\mathbf{NVI = \frac{Channel\ 2 - Channel\ 1}{Channel\ 2 + Channel\ 1}}$$

or

$$\mathbf{NVI = \frac{VI}{Channel\ 2 + Channel\ 1}}$$

The NVI compensates, in part, for changing illumination conditions, the variation in viewing angles and terrain irregularities. Neither the NVI nor the VI compensates for atmospheric effects such as scattering by dust and atmospheric moisture (haze), sub-pixel clouds, etc. These variables act to increase the observed values in Channel 1 and decrease the value of the VI or NVI.

Cloud areas, snow cover, and water surfaces have higher reflectances in the visible than in the near-infrared, thus the computed VI values are negative in these areas. Bare soil and rock areas have about the same reflectance in these channels, and result in an index value near zero. Areas with increasing amounts of vegetative cover have increasingly larger values of VI or NVI.

Depending on user requirements, the vegetation indices may be computed daily, weekly, or monthly. In April 1982, NESDIS began computing a daily NVI from the AVHRR data. These data are mapped into northern and southern hemispheric polar stereographic arrays with a resolution of 15 km at the equator to 30 km at the poles. The NVI values are then composited into weekly (seven day), randomly sampled, maximum NVI files that are available on computer compatible tapes (CCT) or as photographic prints. The compositing process assists in filtering out clouds and particulate contamination and provides a more representative depiction of the vegetation index.

The vegetation index is operationally used by the NESDIS Assessment and Information Services Center (AISC) to assess climatic effects on vegetation and crops. A color coordinate system has been developed for analysis purposes (Ambroziak, 1984). Typical displays produced by this system appear on page 12.

Regional weather and vegetation cover information from the polar-orbiting NOAA satellites can be merged with conventional surface weather reports and local agricultural crop and farming information to provide a valuable analysis package that can be used to assess drought, seasonal crop progress relative to normal, and to estimate crop yields.

Further Reading

Ambroziak, R. A., 1984: Global crop monitoring: an integrated approach. *Proceedings, Recent Advances in Civil Remote Sensing*, May 3–4, 1984, Arlington, VA, International Society for Optical Engineering, Bellingham, WA, **481**, 238–244.

continued on page 12

SEASONAL VEGETATION CHANGES

The following series of NOAA-7 vegetation index (VI) are displayed using the Ambroziak (loc. cit., p. 11) color coordinate system. In this display, (G) denotes fixed geographical features; darker green tones represent increasing amounts of vegetation; and brown tones represent the barren sands and soils of the African Sahel. (V–V′) marks the edge of the vegetation on 27 December 1982 (12-1), 11 July 1983 (12-2), and 9 July 1984 (12-3, from van Dyk, 1984).

Of interest are the slight differences in vegetation progress northward over the Ivory Coast and along the Gulf of Guinea coastal areas. Note, also, that eastern Nigeria (N), Cameroon, Equatorial Guinea, and Gabon (C) are substantially lacking in vegetative cover in July 1984 compared to the previous year (solid line-1983).

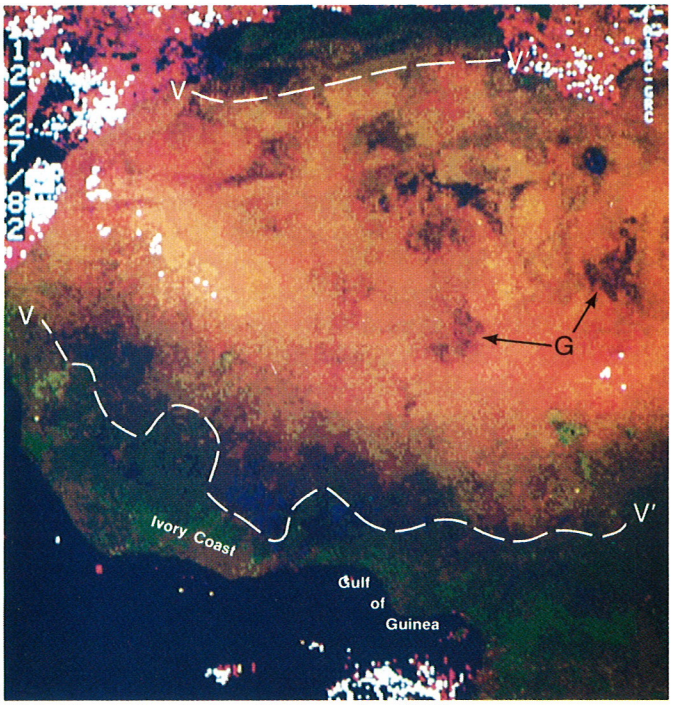

12-1. Vegetation Index. 27 December 1982.

Further Reading

Merritt, E. S., L. Heitkemper, and K. Marcus, 1984: CROPCAST-A review of an existing remote sensor-based agricultural information system with a view toward future remote sensor applications. *Proceedings, Recent Advances in Civil Remote Sensing*, May 3–4, 1984, Arlington, VA, International Society for Optical Engineering, Bellingham, WA, **481**, 231–237.

Schneider, S. R., D. F. McGinnis, and J. A. Gatlin, 1981: Use of NOAA/AVHRR visible and near-infrared data for land remote sensing. NOAA Tech. Rep. NESS 84, U.S. Dept. of Commerce, Washington, D.C., 48 pp.

Tarpley, J. D., S. R. Schneider, and R. L. Money, 1984: Global vegetation indices from the NOAA-7 meteorological satellites. *J. Climate Appl. Meteor.*, **23**, 491–494.

Tucker, C. J., 1978: A comparison of sensor bands for vegetation monitoring. *Photogrammetric Engineering and Remote Sensing*, **44**, 1369–1380.

Tucker, C. J., J. A. Gatlin, and S. R. Schneider, 1984: Monitoring vegetation in the Nile Delta with NOAA-6 and NOAA-7 AVHRR imagery. *Photogrammetric Engineering and Remote Sensing*, **44**, 53–61.

van Dyk, A., D. McCrary, S. LeDuc, and M. Lyn, 1984: *AVHRR Training Set, Volume 1.* NOAA/NESDIS/AISC and University of Missouri, Columbia, MO, 97 pp.

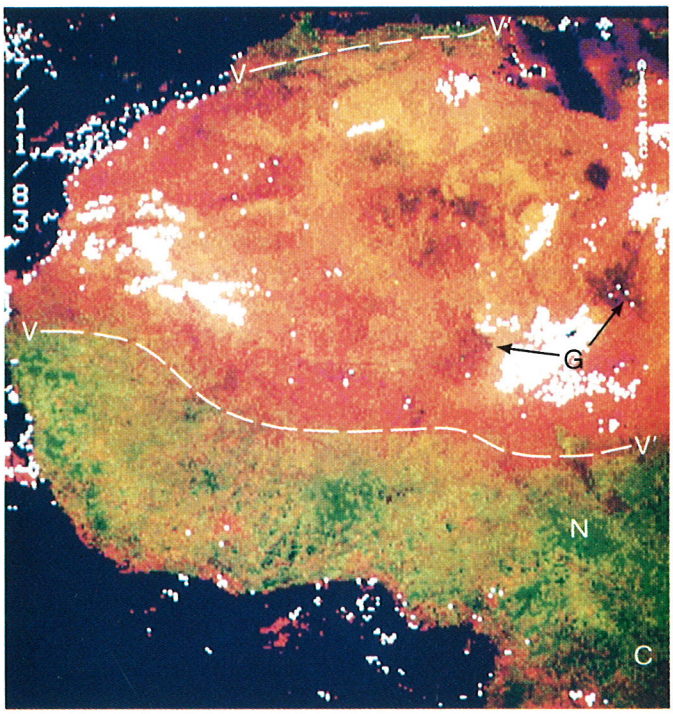

12-2. Vegetation Index. 11 July 1983.

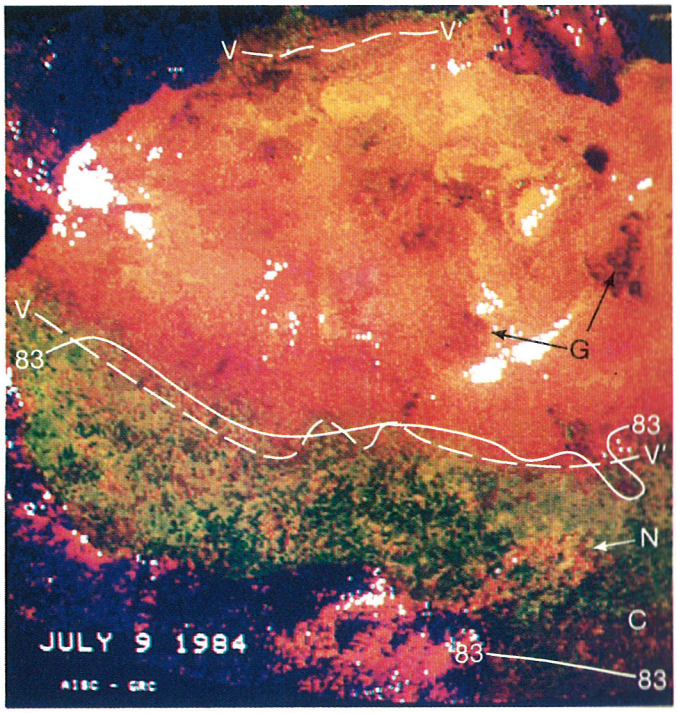

12-3. Vegetation Index. 9 July 1984.

FIRE FUELS MONITORING

Determination of forest and wildland conditions are vital to fire management personnel. Decisions regarding equipment and personnel staging, both in readiness and on-site, can be aided by NOAA polar-orbiting satellite data. The Department of Interior, Bureau of Land Management, has developed a fire fuels monitoring system that merges data bases containing information regarding elevation, slope, aspect, roads, land cover, and fuel types. The vegetation index (VI) derived from Channel 1 and 2 of the AVHRR has proved to be a valuable source for determining land cover and fuel type information. The frequent interval data coverage by the NOAA satellites allows these critical fire fuel conditions to be monitored on an operational basis.

This example of the fire fuels monitoring system was used in the Vale and Burns Districts of eastern Oregon during the spring 1982 fire season (13-1). This computer-generated composite product includes the NOAA AVHRR vegetation index data which has been combined with digital terrain data and surface data from selected ground control points and field sites. Land cover is color coded. The letters in parenthesis represent coding for fuel models as defined by the National Fire Danger Ratings System (NFDRS). Similar maps can be generated to monitor fire fuel buildup and assess the risk of wildfires, estimate the time of maturation of herbaceous vegetation as an indicator of fire potential, and identify and plan for counteractive fire measures.

Further Reading

Miller, W. A., E. P. Chine, and S. M. Howard, 1983: Evaluation of AVHRR data to develop fire fuels information as an input to IAMS. Final Report Contract Y/A-551-CT3-440001, U.S.G.S., Earth Resources Observation Systems (EROS) Data Center, Sioux Falls, SD, 77 pp.

Werth, L., R. McKinely, and R. Franklin, 1984: Use of NOAA satellite data for BLM wildfire fuels mapping in California and Nevada. *Proceeding of Pathways and Future Directions for Environmental Data and Information Users*, August 19–21, 1984, Denver, Colorado, National Environmental Satellite, Data, and Information Service, Washington, D.C., 362–371.

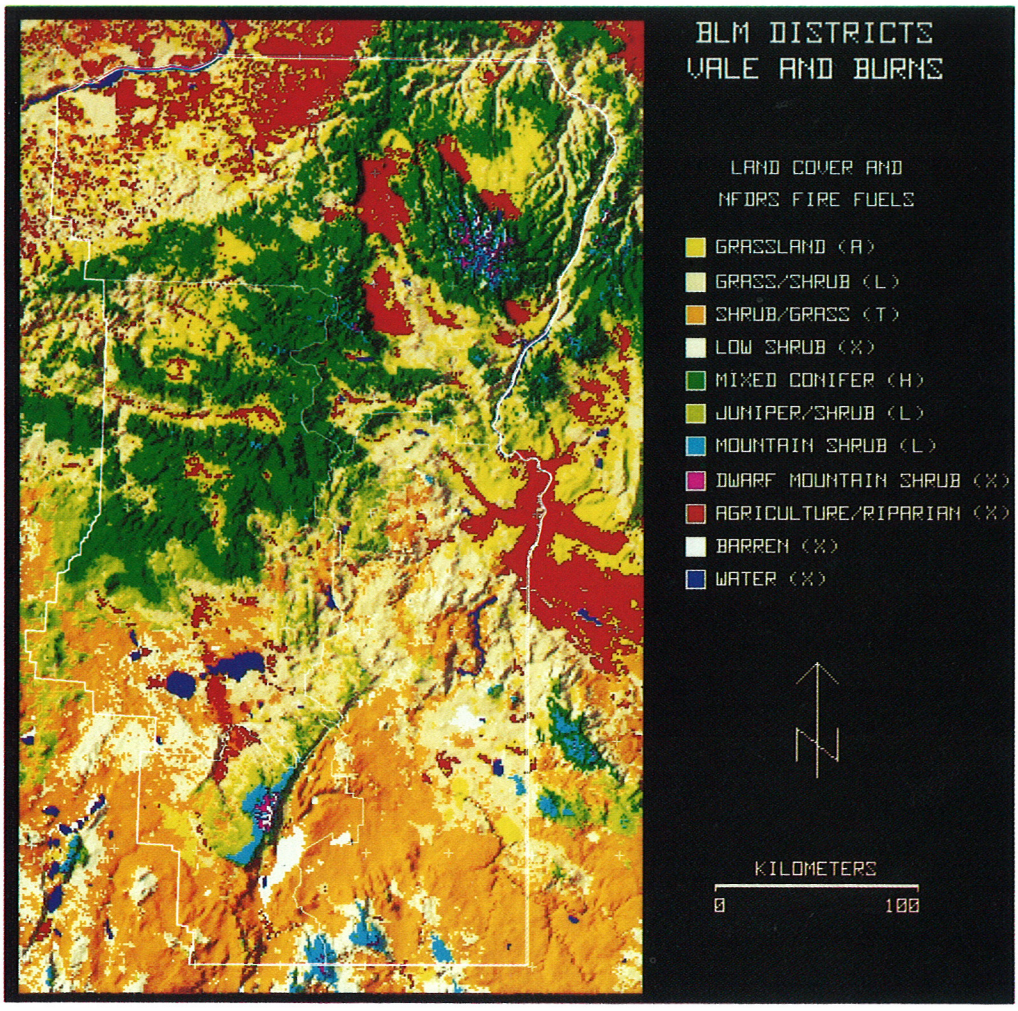

13-1. BLM Districts, Vale and Burns. Land Cover and NFDRS Fire Fuels Assessment. (from Miller et al., 1983)

Eastern Oregon Study Area

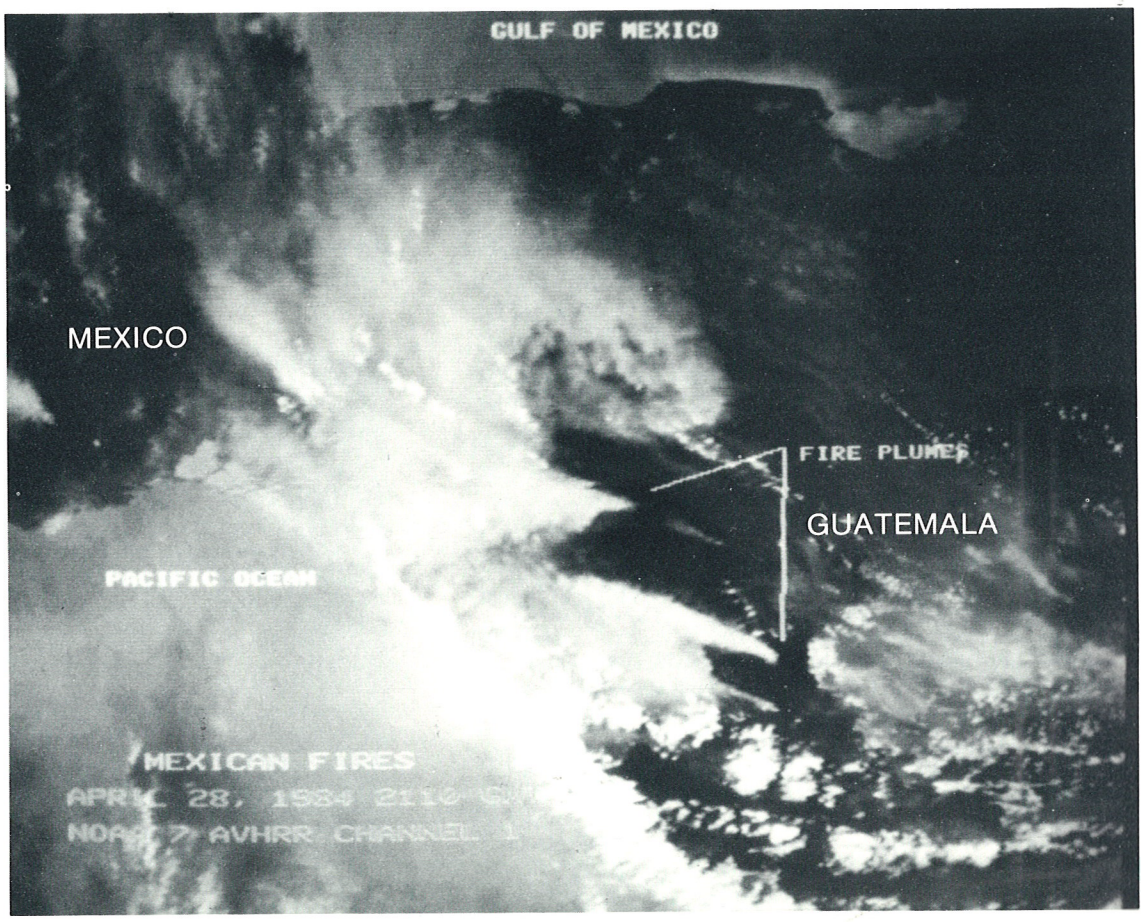

14-1. NOAA-7.
Visible Image.
28 April 1984.

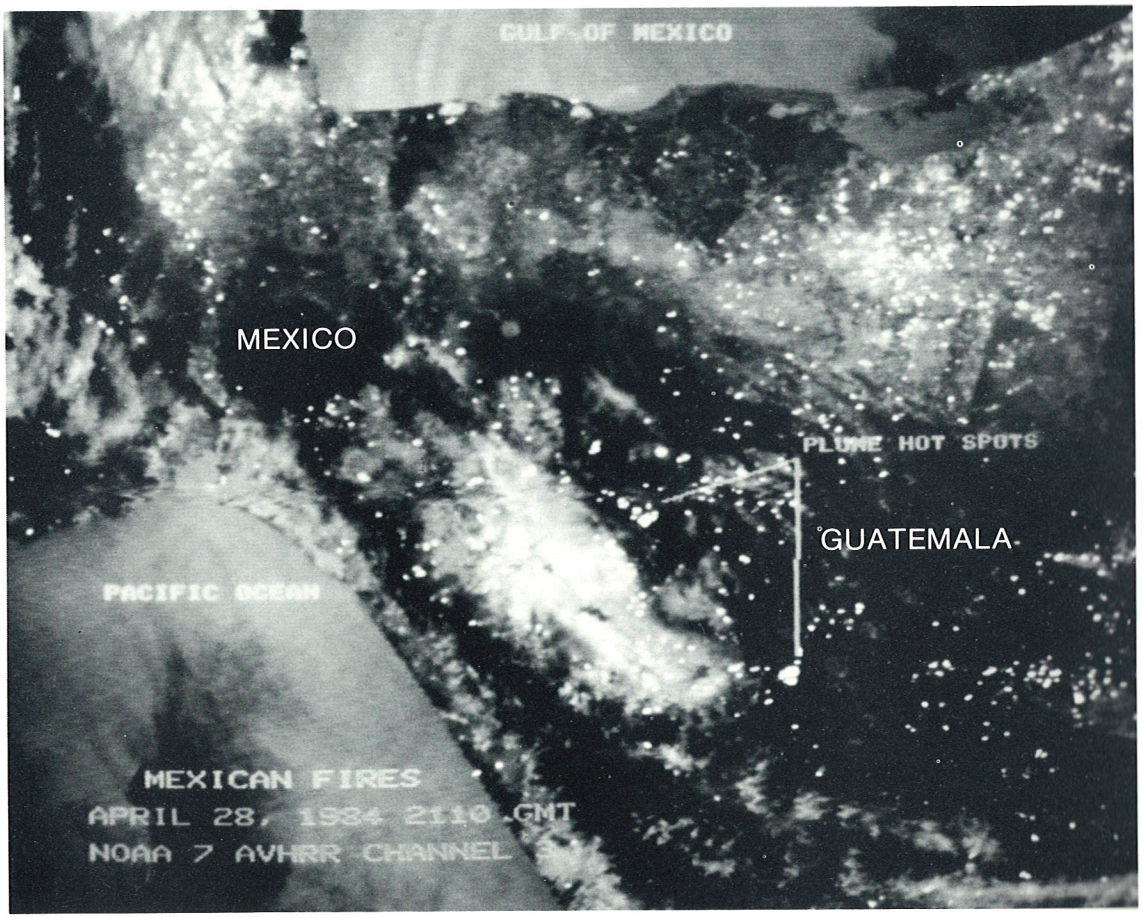

14-2. NOAA-7.
Thermal mid-Infrared
Image.
28 April 1984.

FIRE DETECTION

An example of the fire detection capability of the NOAA polar-orbiting series of satellites is shown on the opposite page (14-1). This computer-enhanced visible band image of southern Mexico and Guatemala taken on 28 April 1984 shows two large fire (smoke) plumes that cover most of the region. The smoke plumes are a result of seasonal slash-and-burn agricultural activities. Although the visible band channel is useful for the analysis of the smoke plume coverage, it is the 3.8 μm channel (Channel 3) that is best for pinpointing the fire areas. This channel is very sensitive to high temperature targets such as fires, which, depending on the display that is used, will appear as white or black "hot spots" on an image. A computer-enhanced 3.8 μm image of 14-1 is shown in 14-2. Over 300 "hot spots" (white dots), associated with the slash-and-burn activity, are apparent on this image. The large white area near the center of the image is the Grijalva Valley, an area of widespread burning. Although this valley is obscured by smoke in the visible band channel, the 3.8 μm sensor penetrates the smoke, which is primarily composed of small particulates and water vapor, to reveal the fire areas.

FIRE MONITORING

In addition to detecting fires, the 3.8 μm channel can also be used to monitor fire movement. A 3X enlargement of the NOAA polar-orbiting satellite data over Dune Lake, Alaska (15-1, 15-2, and 15-3), taken over the period 22–24 May 1981, illustrates this. (In this display black represents hot areas and white, cold areas). Thunderstorm activity initiated the Dune Lake fire on 15 May. By 22 May (15-1), the fire covered 75,000 acres, and was most intense along the southeast (black area) front. These scenes show that the hottest or most intense fire areas progressed from south to north, and the total burnt area (dark gray) increased eastward during this three-day period. Satellite data combined with meteorological observations and forecasts can be valuable tools for operational fire management.

Further Reading

Ernst, J. A., and M. Matson, 1977: A NOAA-5 view of Alaska smoke patterns. *Bull. Amer. Meteor. Soc.*, **58**, 1074–1076.

Jayaweera, K. O. L. F., and K. Ahlnas, 1974: Detection of thunderstorms from satellite imagery for forest fire control. *J. of Forestry*, **72**, 767–770.

Matson, M., and J. Dozier, 1981: Identification of subresolution high temperature sources using a thermal IR sensor. *Photogrammetric Engineering and Remote Sensing*, **47**, 1311–1318.

Matson, M., S. R. Schneider, B. Aldridge, and B. Satchwell, 1984: Fire detection using the NOAA-series satellites. NOAA Tech. Rep. NESDIS 7, U.S. Dept. of Commerce, Washington, D. C., 34 pp.

Parmenter, F. C., 1971: Smoke from slash burning operations. *Mon. Wea. Rev.*, **99**, 684–685.

Parmenter, F. C., 1977: Convective cloud plumes mark Canadian fire sites. *Weather*, **32**, 424–427.

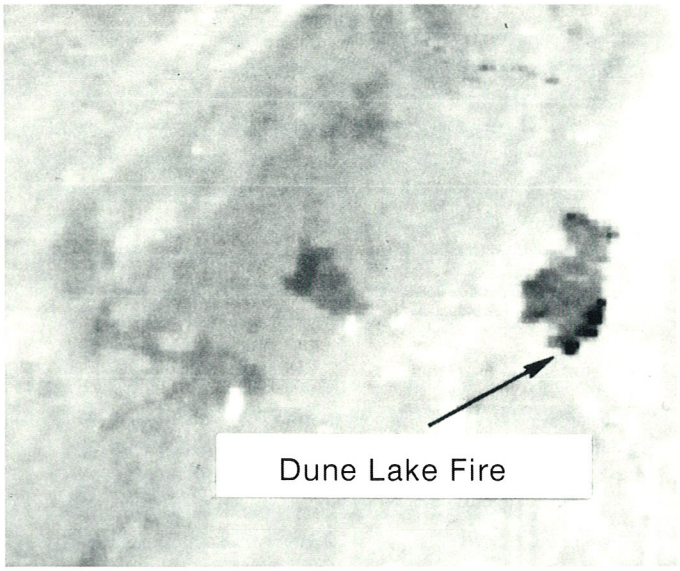

15-1. NOAA-6. Thermal mid-Infrared. 22 May 1981.

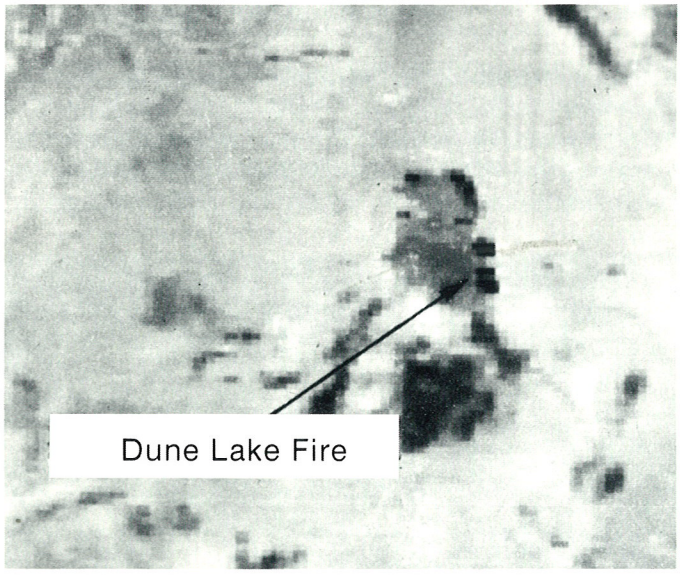

15-2. NOAA-6. Thermal mid-Infrared. 23 May 1981.

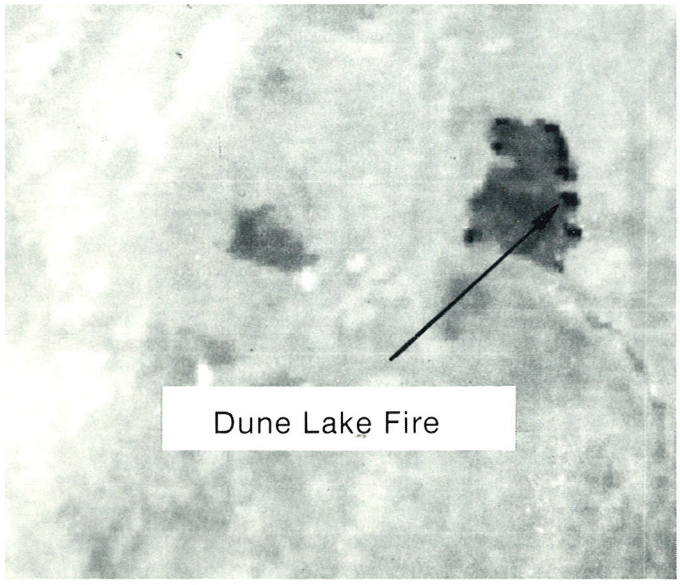

15-3. NOAA-6. Thermal mid-Infrared. 24 May 1981.

URBAN EFFECTS

Applications of the vegetation index to agricultural and forest management activities have been previously addressed. The vegetation index can also be used to monitor regional land use and urban growth. This pair of AVHRR images (16-1 and 16-2) was simultaneously acquired over the eastern mid-Atlantic United States on 21 July 1982 and depict the normalized vegetation index (NVI) and the thermal infrared scene, respectively.

Increasingly darker tones in the NVI (16-1) represent actively growing areas such as the forested ridges of the Appalachians (A–A′). Alternating with the mountain ridges are long valley areas where land is used for farming and grazing. Note that in the thermal infrared image (16-2), the forested areas are cooler (lighter gray) and the valley (S–S′) is warmer. This is due primarily to the elevation differences of these areas.

The urban sites of Baltimore, Maryland (BAL), Washington, D.C. (DCA), Richmond, Virginia (RIC), and Norfolk and Newport News, Virginia (N) appear as very warm (dark) areas in the thermal infrared (16-2) and without substantive vegetation (lighter grays) in the NVI (16-1). Comparison of imagery over five- or ten-year intervals could provide useful information for regional land-use planners and may also be of interest to scientists studying local climatologies.

The Susquehanna River (R) and the coves and inlets surrounding Chesapeake and Delaware Bays are also visible. Note that these features are more prominent in the NVI image than in the thermal infrared. Since water appears nearly the same in the visible and near-infrared, the NVI is zero and is displayed as very light gray. Since this scene was taken during the summer, rivers and inlets have nearly the same temperatures as the land, thus those features are not as easily detectable in the daytime thermal infrared image.

Further Reading

Carlson, T. N., J. N. Augustine, and F. E. Boland, 1977: Potential application of satellite temperature measurements in the analysis of land use over urban areas. *Bull. Amer. Meteor. Soc.*, **58**, 1301–1303.

Landsberg, H. E., 1970: Man-made climatic changes. *Science*, **170**, 1265–1274.

Matson, M., E. P. McClain, D. F. McGinnis, Jr., and J. A. Pritchard, 1978: Satellite detection of urban heat islands. *Mon. Wea. Rev.*, **105**, 1725–1734.

16-1. NOAA-7 AVHRR normalized vegetation index (NVI) over the eastern mid-Atlantic States at 1952 GMT 21 July 1982.

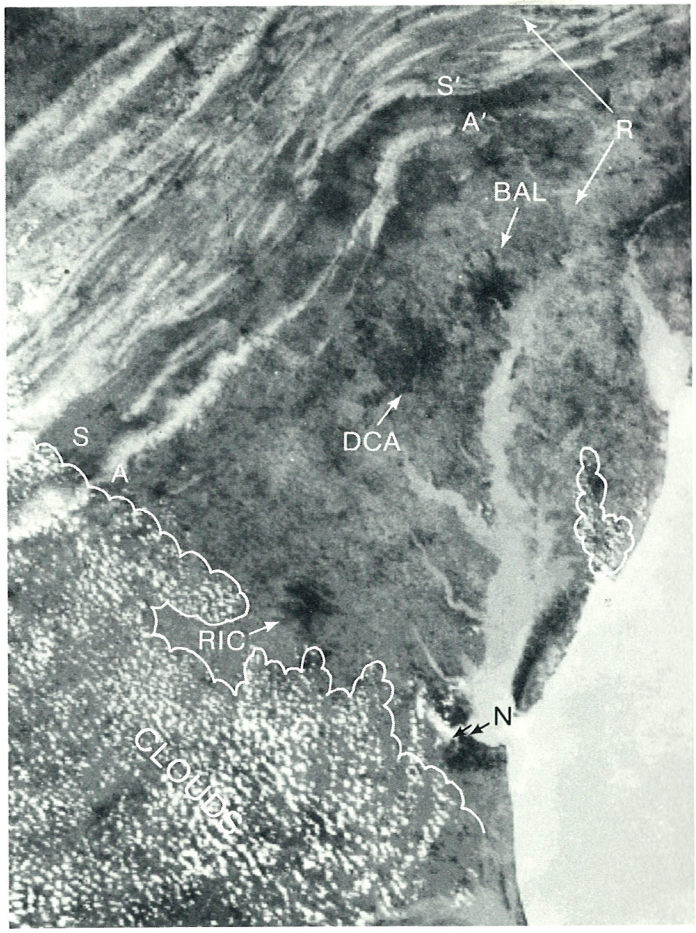

16-2. NOAA-7 AVHRR thermal infrared image over the eastern mid-Atlantic States at 1952 GMT 21 July 1982.

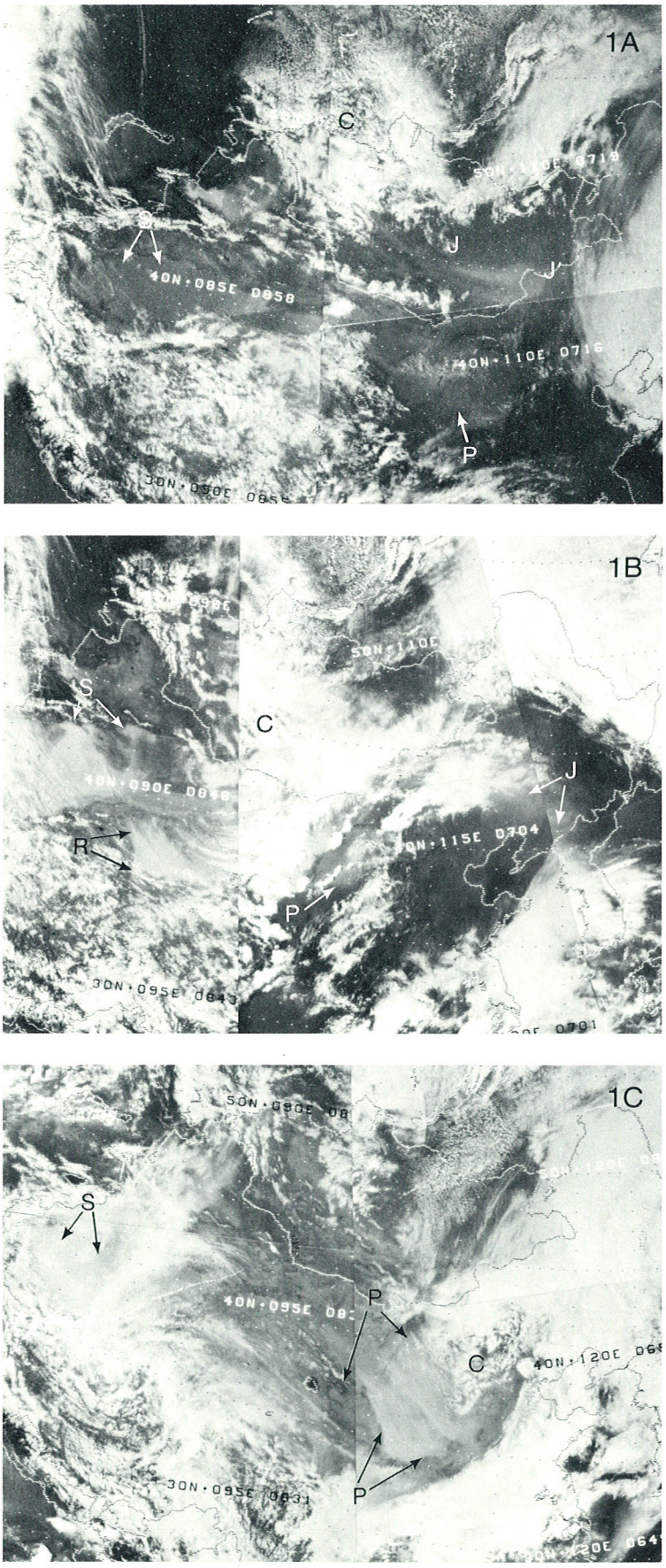

17-1. Mosiac of NOAA-7, GAC visible data taken at (1A) 0730–0912 GMT 26 April 1983, (1B) 0530–0900 GMT 27 April 1983, and (1C) 0705–0847 GMT 28 April 1983.

Airborne dust and sand present serious problems to vehicular traffic both on the ground and in the air. Dust and sandstorms are frequently observed in the mid-latitudes during the spring when strong weather systems or thunderstorms traverse desert or barren soil areas. The resulting suspended dust layer or cloud can cover thousands of miles. Occasionally the airborne dust and sand enter into the initiating weather system and "mud" or yellow rains are observed far from the origin of the dust or sand.

Visible satellite imagery can be used to identify sources and areal coverage of this phenomenon. Most desert soils are light in color, and when airborne, the suspended dust cloud may appear similar to fog or dense cirrus. Familiarity with the clear sky appearance of terrain features of dust and sandstorm areas is key to analyzing and monitoring a duststorm event.

A number of duststorms can be seen in this sequence of NOAA-7, Global Area Coverage (GAC) data (17-1A, 1B, and 1C), taken of China and Mongolia from 26–28 April 1983. Frequently the dust cloud is observed with a definite point source that expands or fans out downwind such as (J–J') in 17-1A and (R) in 17-1B. In other cases such as in the Sinkiang Desert (S, 17-1A, 1B, and 1C), airborne dust appears amorphous. Typically, after the thunderstorms or weather fronts have passed and the winds have subsided, the dust area loses shape and brightness.

Of particular interest in this series is the approach of the storm (C) in 17-1A and 1B, and the initiation of a dust area at (P). A train traveling from Beijing (Peking) to Urumqi through the Gobi Desert area experienced strong winds that blew out 60 windows and halted the train for six hours on 27 April (17-1B)[2]. The large dust area generated by this storm can be seen at (P, 17-1C), and covers more than 1000 square miles.

[2] Associated Press reports—Gobi Desert Windstorm Stops Train–All Passengers Safe.

Further Reading

Carlson, T., and J. Prospero, 1972: The large-scale movement of Saharan air outbreak over the northern Equatorial Atlantic. *J. Appl. Meteor.*, **11**, 283–297.

D'Aguanno, J. A., 1983: 1982 Saharan dust outbreak. *Mar. Wea. Log.*, **27**, 199–200.

Otterman, J., 1981: Studies of duststorms from satellites. In *Remote Sensing in Meteorology, Oceanography, and Hydrology*, edited by A. P. Cracknell, Ellis Howard, Pub, Ltd., 249–257.

Shenk, W. E., and R. J. Curran, 1974: Detection of duststorms over land and water with satellite visible and infrared measurement. *Mon. Wea. Rev.*, **102**, 830–837.

VOLCANOES

Because of their global and frequent coverage, the NOAA polar-orbiting satellites are excellent platforms for observing volcanic eruptions, especially in remote parts of the world. The multispectral polar-orbiting data can be used to determine the vertical and horizontal plume morphology, track the ash cloud trajectory, monitor the eruption growth rate, and calculate the plume altitude.

The NOAA visible image (18-1) shows the Alaid eruption south of the Kamchatka Peninsula in the Soviet Union on 29 April 1981. A nearly 90° difference in the orientation of the low- and high-level plume can be seen, suggesting strong low-level wind shear in this area. Computer enhancement of the simultaneously acquired thermal infrared channel data (18-2) shows distinct temperature differences between the two plumes. By comparing the satellite-derived temperatures to nearby radiosonde data (temperature versus height), it is possible to determine the maximum altitude of the high-level plume. In this case the lowest satellite-observed temperature of −65° C corresponded to an altitude of 12 km. A similiar analysis for the Mt. Etna, Sicily, eruption on 15 May 1983 (18-3) gave a satellite-observed temperature of −33° C, corresponding to a height of 5 km.

In addition to their use in volcanological studies, the satellite data may be useful in issuing warnings to aircraft flying near erupting volcanoes. In June and July of 1982, two Boeing 747 aircraft flew into ash clouds from the erupting Galunggung volcano in Java. Both suffered multiple engine failures and severe losses of altitude. Fortunately, safe emergency landings were made with no injuries. These near-fatal incidents have prompted the International Civil Aeronautics Organization to examine the possibility of using satellite data to provide ash cloud warnings to pilots when a volcano erupts.

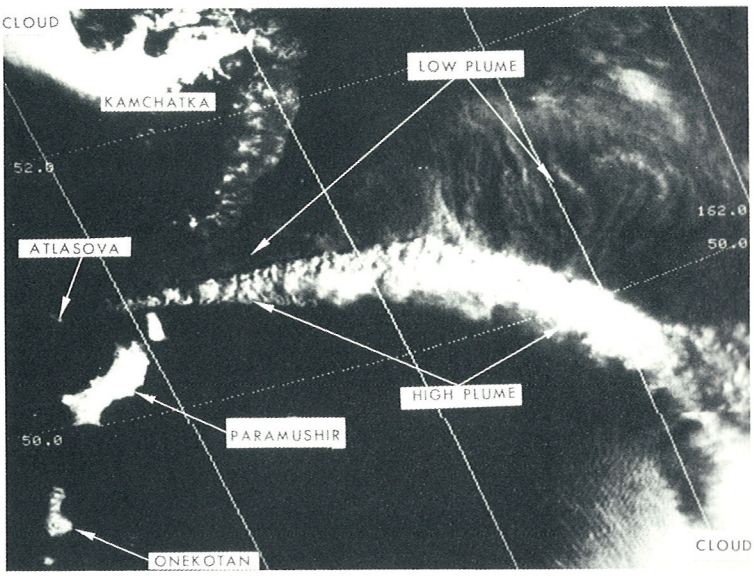

18-1. NOAA-6. Visible Image. 29 April 1981.

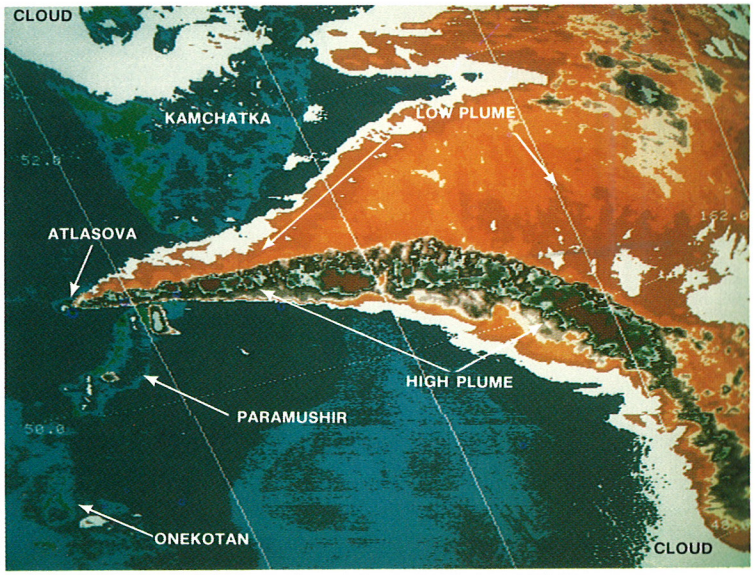

18-2. NOAA-6. Thermal Infrared Image. 29 April 1981.

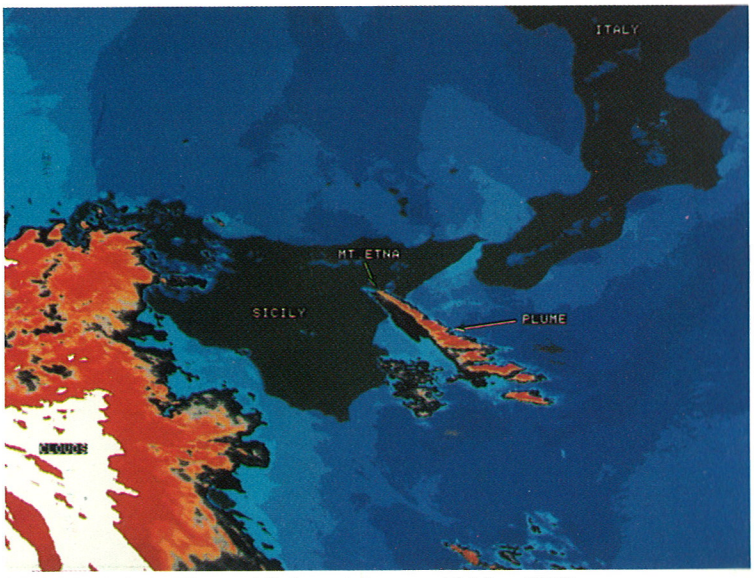

18-3. NOAA-7. Thermal Infrared Image. 15 May 1983.

Further Reading

Kienle, J., and G. E. Shaw, 1979: Plume dynamics, thermal energy and long distance transport of vulcanian eruption clouds from Augustine Volcano, Alaska. *J. of Volcanology and Geothermal Res.*, **6**, 139–164.

Krueger, A. F., 1980: Satellite observations: the Soufriere Volcano. *Weatherwise*, **33**, 71–74.

Robock, A., and M. Matson, 1983: Circumglobal transport of the El Chichon volcanic dust cloud. *Science*, **221**, 195–197.

GEOLOGIC ASSESSMENT

Researchers at the Smithsonian Institution have examined the use of AVHRR, multispectral thermal infrared data for mapping tectonic features of a geologic site on the Arabian Peninsula (19-1). The study area includes two distinct geologic types: igneous and metamorphic rocks in the eastern portion of the Arabian/Nubian Shield, and a succession of arcuate north–south trending exposures of sedimentary formations that dip eastward at less than 5°. The region of valley fill between the two geologic types contains a well-defined 7- to 45-km wide band of alluvium and eolian sands. The Najd Fault system extends southeastward more than 1,000 km from the Red Sea to its terminus at the eastern edge of the shield.

A computerized composite (19-2) was produced from day and night temperature ratios from the NOAA AVHRR Channels 3, 4, and 5. In this colored display, low ratio values (small day/night temperature changes) appear dark and high ratio values (large day/night temperature changes) appear light. Thus light areas readily release the radiant energy absorbed during the daytime, whereas dark areas do not. These and other intermediate differences are then related to lithologic features.

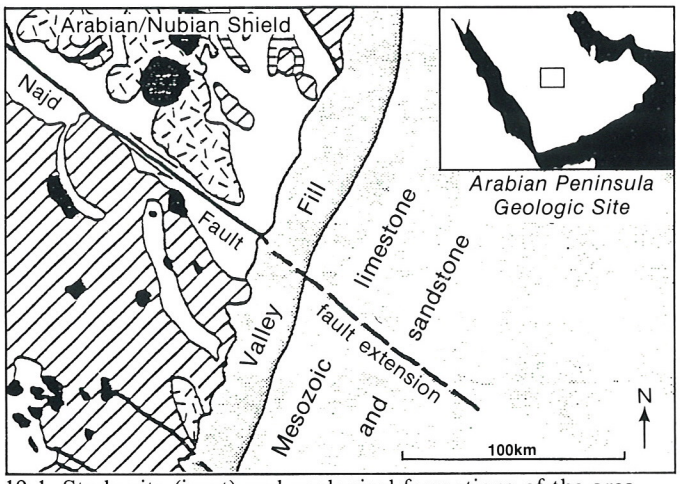

19-1. Study site (inset) and geological formations of the area.

For example, granite intrusions appear as roughly circular black features (coordinates D.7, 2.4, and D.3, 2.2) because they retain heat more efficiently than surrounding surfaces. On the other hand, the S-shaped anhydrite outcrop (coordinates C.3, 5.0) is a light hue of red (large daytime heat release) relative to the adjacent gravels that appear as dark blue areas (daytime heat retention). The dark blue unit that trends northeast to southwest (coordinates A.0, 2.9, to E.0, 4.4) correlates to gravels at the western margin of the Mesozoic limestone and sandstone formations in the right half of the picture. Nearly orthogonal to the trend of these formations is a prominent thermal lineament that lies northwest to southeast (arrows on border of 19-2), and extends a distance of more than 300 km. In the shield area, the lineament appears white and accurately traces the line of the Najd Fault. The remainder of the lineament extends eastward almost 200 km. It is believed that this lineament denotes a newly discovered extension of the Najd Fault, an extension not detected using higher resolution Landsat visible and near-infrared imagery or with conventional field mapping techniques.

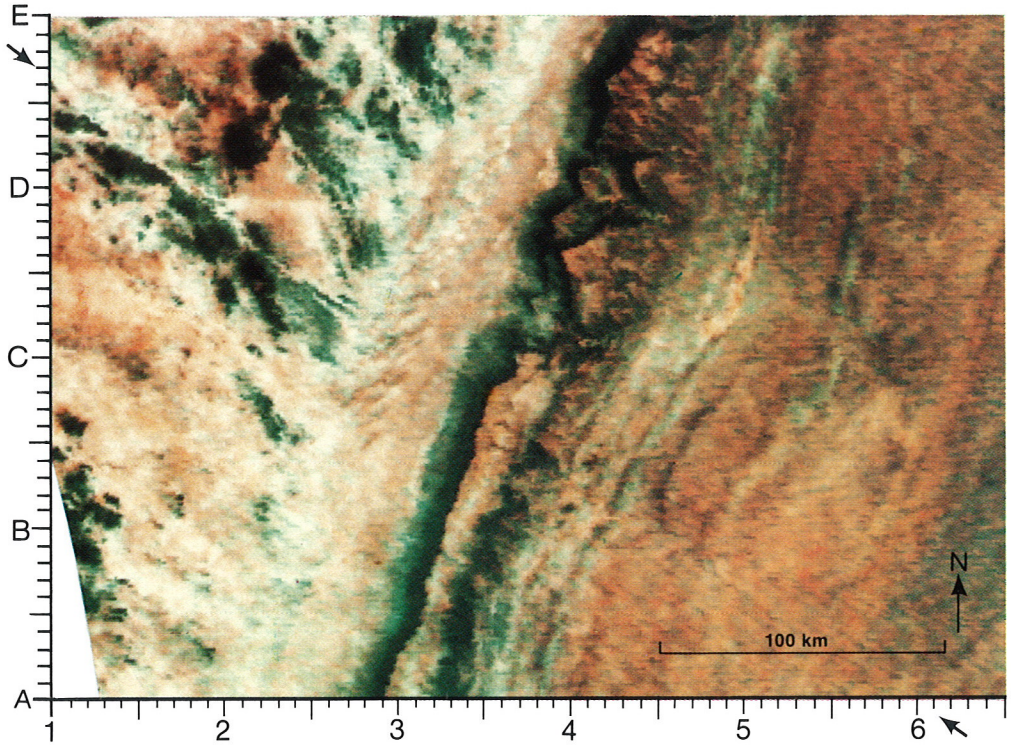

19-2. Computerized composite of day and night temperature ratios from the NOAA AVHRR, Channels 3, 4, and 5. (From Andre and Blodget, 1984.)

Further Reading

Andre, C. G., and H. W. Blodget, 1984: Thermal infrared satellite data for the study of tectonic features. *Geophysical Res. Letters*, **11**, 983–986.

Schneider, S. C., D. F. McGinnis, and J. A. Pritchard, 1979: Delineation of drainage and physiographic features in North and South Dakota using NOAA-5 infrared data. In *Satellite Hydrology*, edited by M. Deutsch, D. R. Wiesnet, and A. Rango, American Water Resources Association, Minneapolis, MN, 324–330.

EPILOGUE

In the preceding pages, we have illustrated a variety of hydrologic and land sciences applications of NOAA polar-orbiting satellite data. As the last example illustrates (page 19), computer technology and multispectral sensor data will be integral to future operations, applications, and advancements. We hope that the brief descriptions in this publication will serve your programs, projects, and plans. For more information, contact:

User Affairs Unit, Code E/ER2
NOAA/National Environmental Satellite, Data, and Information Service
Federal Building #4 Room 3301 Stop D
Washington, D.C. 20233

ACKNOWLEDGEMENTS

The authors wish to thank Ralph K. Anderson, Satellite Applications Laboratory, for his technical assistance and review.

Other NOAA Programs of Interest

DATA COLLECTION SERVICES

Collection of real-time or near real-time data (e.g. river stage, snow gauge, seismological, temperature, etc.) from surface-based platforms is a service available to hydrologists and land scientists. A number of reporting modes, such as self-timed, interrogated, emergency, or random, can be employed to relay environmental data back to users. Data collection services are available on both the NOAA operated polar-orbiting and geostationary (Western Hemisphere) satellites. For further information, contact:

Service ARGOS
U.S. Office
Federal Building #4
Suitland, Maryland 20233
U.S.A. Ref-HLSB Project

International Office
Centre National D'Etudes Spatiale
18 AV Edouard-Belin
31055 Toulouse Cedex
FRANCE Ref-HLSB Project

Geostationary Program (Western Hemisphere)
Data Collection and Distribution Branch
NOAA/National Environmental Satellite, Data, and Information Service
HLSB Project, Code E/SP21 Stop I
World Weather Building Room 806
Washington, D.C. 20233

DIRECT BROADCAST SERVICES

Information concerning local acquisition of polar-orbiting satellite data may be obtained from:

Satellite Program Specialist
NOAA/National Environmental Satellite, Data, and Information Service
HLSB Project
User Affairs Unit, Code E/ER2
Federal Building #4 Room 3301 Stop D
Washington, D.C. 20233

NOAA SATELLITE DATA ARCHIVAL PRODUCTS

Retrospective data from the polar-orbiting satellites are available in photographic and computer compatible tape (CCT) formats. Ordering information is available from:

Satellite Data Service Branch
NOAA/National Environmental Satellite, Data, and Information Service
HLSB Project, Code E/CC6
World Weather Building Room 100
Washington, D.C. 20233

Back Cover:

Northwest Canada
NOAA-5, 15 March 1978
Visible Image

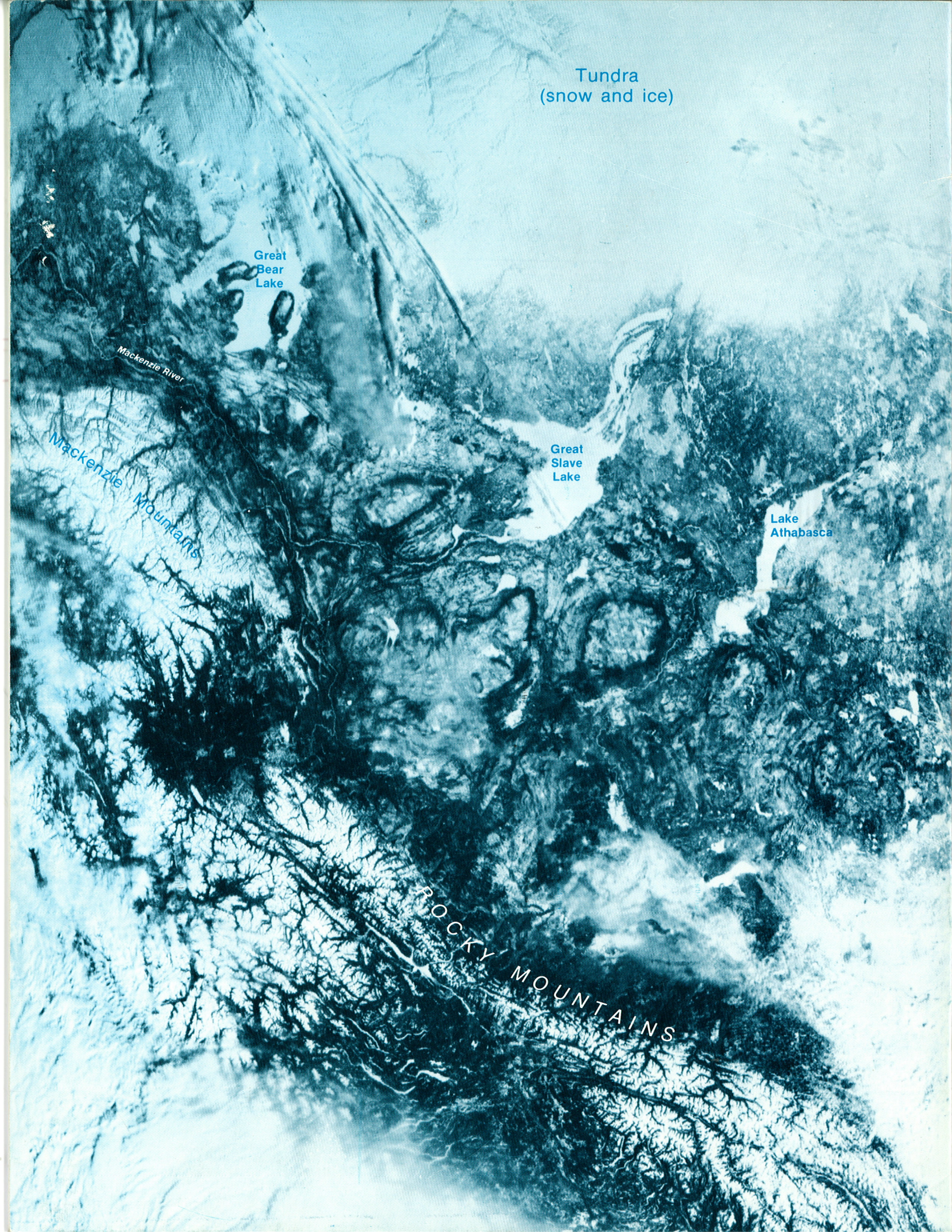
Tundra
(snow and ice)
Great
Bear
Lake
Mackenzie River
Mackenzie Mountains
Great
Slave
Lake
Lake
Athabasca
ROCKY MOUNTAINS